

Low energy hadron physics with carlomat_3.0

Karol Kołodziej

Institute of Physics
University of Silesia
Katowice

XXXIX International Conference of Theoretical Physics
MATTER TO THE DEEPEST:
Recent Developments in Physics of Fundamental Interactions
Ustroń, 13-18 September, 2015

The knowledge of $\sigma_{e^+e^- \rightarrow \text{hadrons}}(s)$ allows, through dispersion relations, for determination of **hadronic contributions to the vacuum polarization**.

⇒ Better precision of theoretical predictions for the **muon anomaly** and **evolution of the fine structure constant** from the Thomson limit to high energy scales. [$\sim 10^{13}$ Z's at e^+e^- collider]

The knowledge of $\sigma_{e^+e^- \rightarrow \text{hadrons}}(s)$ allows, through dispersion relations, for determination of **hadronic contributions to the vacuum polarization**.

⇒ Better precision of theoretical predictions for the **muon anomaly** and **evolution of the fine structure constant** from the Thomson limit to high energy scales. [$\sim 10^{13}$ Z's at e^+e^- collider]

Below the J/ψ threshold, $\sigma_{e^+e^- \rightarrow \text{hadrons}}(s)$ must be measured, either by the **initial beam energy scan** or with the use of a **radiative return method**, and compared with predictions of a Monte Carlo program, as e.g. PHOKARA. [Czyż, Kühn, et al.]

The knowledge of $\sigma_{e^+e^- \rightarrow \text{hadrons}}(s)$ allows, through dispersion relations, for determination of **hadronic contributions to the vacuum polarization**.

⇒ Better precision of theoretical predictions for the **muon anomaly** and **evolution of the fine structure constant** from the Thomson limit to high energy scales. [$\sim 10^{13}$ Z 's at e^+e^- collider]
Below the J/ψ threshold, $\sigma_{e^+e^- \rightarrow \text{hadrons}}(s)$ must be measured, either by the **initial beam energy scan** or with the use of a **radiative return method**, and compared with predictions of a Monte Carlo program, as e.g. PHOKARA. [Czyż, Kühn, et al.]

To reach the desired precision level, radiative corrections must be included in the predictions for the dominant hadronic channels.

The knowledge of $\sigma_{e^+e^- \rightarrow \text{hadrons}}(s)$ allows, through dispersion relations, for determination of **hadronic contributions to the vacuum polarization**.

⇒ Better precision of theoretical predictions for the **muon anomaly** and **evolution of the fine structure constant** from the Thomson limit to high energy scales. [$\sim 10^{13}$ Z 's at e^+e^- collider]
Below the J/ψ threshold, $\sigma_{e^+e^- \rightarrow \text{hadrons}}(s)$ must be measured, either by the **initial beam energy scan** or with the use of a **radiative return method**, and compared with predictions of a Monte Carlo program, as e.g. PHOKARA. [Czyż, Kühn, et al.]

To reach the desired precision level, **radiative corrections must be included in the predictions for the dominant hadronic channels**.
However, it is probably enough to have the LO predictions for channels with smaller cross sections.

The knowledge of $\sigma_{e^+e^- \rightarrow \text{hadrons}}(s)$ allows, through dispersion relations, for determination of **hadronic contributions to the vacuum polarization**.

⇒ Better precision of theoretical predictions for the **muon anomaly** and **evolution of the fine structure constant** from the Thomson limit to high energy scales. [$\sim 10^{13}$ Z 's at e^+e^- collider]
Below the J/ψ threshold, $\sigma_{e^+e^- \rightarrow \text{hadrons}}(s)$ must be measured, either by the **initial beam energy scan** or with the use of a **radiative return method**, and compared with predictions of a Monte Carlo program, as e.g. PHOKARA. [Czyż, Kühn, et al.]

To reach the desired precision level, radiative corrections must be included in the predictions for the dominant hadronic channels. However, it is probably enough to have the LO predictions for channels with smaller cross sections.

The most promising theoretical frameworks for the description of $e^+e^- \rightarrow$ hadrons at low energies are the Resonance Chiral Theory or Hidden Local Symmetry model which, among others, involve

- the photon–vector meson mixing
- a number of vertices of a rather complicated Lorentz tensor structure that is not present in the Standard Model or scalar QED.

Already at low energies, the hadronic final states may consist of several particles, such as pions, kaons, or nucleons which can be accompanied by one or more photons, or light fermion pairs such as e^+e^- , or $\mu^+\mu^-$.

The most promising theoretical frameworks for the description of $e^+e^- \rightarrow$ hadrons at low energies are the Resonance Chiral Theory or Hidden Local Symmetry model which, among others, involve

- the photon–vector meson mixing
- a number of vertices of a rather complicated Lorentz tensor structure that is not present in the Standard Model or scalar QED.

Already at low energies, the hadronic final states may consist of several particles, such as pions, kaons, or nucleons which can be accompanied by one or more photons, or light fermion pairs such as e^+e^- , or $\mu^+\mu^-$.

The number of Feynman diagrams of such multiparticle reactions grows substantially with increasing numbers of interaction vertices and mixing terms of the effective models.

⇒ It is highly desirable to automatize the calculations.

The most promising theoretical frameworks for the description of $e^+e^- \rightarrow$ hadrons at low energies are the Resonance Chiral Theory or Hidden Local Symmetry model which, among others, involve

- the photon–vector meson mixing
- a number of vertices of a rather complicated Lorentz tensor structure that is not present in the Standard Model or scalar QED.

Already at low energies, the hadronic final states may consist of several particles, such as pions, kaons, or nucleons which can be accompanied by one or more photons, or light fermion pairs such as e^+e^- , or $\mu^+\mu^-$.

The number of Feynman diagrams of such multiparticle reactions grows substantially with increasing numbers of interaction vertices and mixing terms of the effective models.

⇒ It is highly desirable to automatize the calculations.

Program `carlomat` has been substantially modified in order to

- incorporate a photon–vector meson mixing,
- include the Feynman interaction vertices of new tensor structures, [provided by F. Jegerlehner]
- to compute the helicity amplitudes involving the mixing terms and new interaction vertices, like those predicted by the $R\chi T$ or HLS model and the effective Lagrangian of the EM interaction of nucleons,
- introduce new options to enable a better control over the effective models implemented.

K. Kołodziej, `carlomat_3.0`, *an automatic tool for the electron-positron annihilation into hadrons at low energies*, Computer Physics Communications (2015),

<http://dx.doi.org/10.1016/j.cpc.2015.06.013> [arXiv:1504.05915]

allows to generate automatically the Monte Carlo programs dedicated to the description of processes $e^+e^- \rightarrow$ hadrons at low centre of mass energies.

Program `carlomat` has been substantially modified in order to

- incorporate a photon–vector meson mixing,
- include the Feynman interaction vertices of new tensor structures, [provided by F. Jegerlehner]
- to compute the helicity amplitudes involving the mixing terms and new interaction vertices, like those predicted by the $R\chi T$ or HLS model and the effective Lagrangian of the EM interaction of nucleons,
- introduce new options to enable a better control over the effective models implemented.


K. Kołodziej, `carlomat_3.0`, *an automatic tool for the electron-positron annihilation into hadrons at low energies*, Computer Physics Communications (2015),

<http://dx.doi.org/10.1016/j.cpc.2015.06.013> [arXiv:1504.05915]

allows to generate automatically the Monte Carlo programs dedicated to the description of processes $e^+e^- \rightarrow$ hadrons at low centre of mass energies.

q^2 -dependent mixing terms

In spite of being conceptually quite simple, the implementation of particle mixing required substantial changes in the code generation part of the program.


$$A^\mu(q) \quad V^\nu(q) \quad \equiv \quad -ef_{AV}(q^2) g^{\mu\nu},$$


with $V = \rho^0, \omega, \phi, \rho_1 = \rho(1450), \rho_2 = \rho(1700)$.

The mixing term introduces an extra power of $e \Rightarrow$ it should be included only once in a Feynman diagram.

q^2 -dependent mixing terms

In spite of being conceptually quite simple, the implementation of particle mixing required substantial changes in the code generation part of the program.

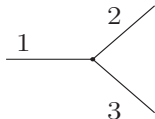
$$A^\mu(q) \quad V^\nu(q) \quad \equiv \quad -ef_{AV}(q^2) g^{\mu\nu},$$


with $V = \rho^0, \omega, \phi, \rho_1 = \rho(1450), \rho_2 = \rho(1700)$.

The mixing term introduces an extra power of $e \Rightarrow$ it should be included only once in a Feynman diagram.

Topology generation in carlomat

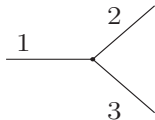
Topologies are generated for models with **triple** and **quartic** couplings, starting with **1 topology** of a **3 particle** process.



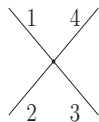
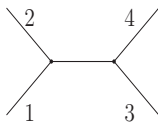
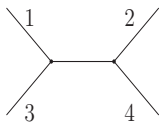
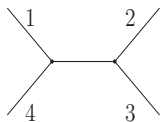
Line 4 is attached to **each line** and to **the vertex** \Rightarrow **4 topologies** of a **4 particle** process.

Topology generation in carlomat

Topologies are generated for models with **triple** and **quartic** couplings, starting with **1 topology** of a **3 particle** process.

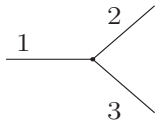


Line 4 is attached to **each line** and to **the vertex** \Rightarrow **4 topologies** of a **4 particle** process.

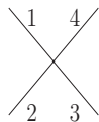
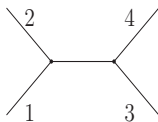
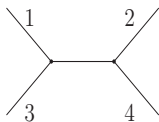
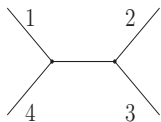


Topology generation in carlomat

Topologies are generated for models with **triple** and **quartic** couplings, starting with **1 topology** of a **3 particle** process.



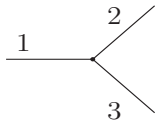
Line 4 is attached to **each line** and to **the vertex** \Rightarrow **4 topologies** of a **4 particle** process.



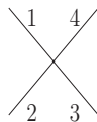
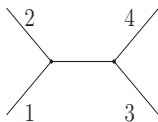
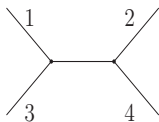
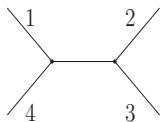
Line 5 is attached to **each line**, including the internal ones, and to each **triple vertex** \Rightarrow **25 topologies** of a **5 particle** process.

Topology generation in carlomat

Topologies are generated for models with **triple** and **quartic** couplings, starting with **1 topology** of a **3 particle** process.



Line 4 is attached to **each line** and to **the vertex** \Rightarrow **4 topologies** of a **4 particle** process.



Line 5 is attached to **each line**, including the internal ones, and to each **triple vertex** \Rightarrow **25 topologies** of a **5 particle** process.

Topology generation in carlomat

of topologies grows dramatically with # of external particles.

# of particles	# of topologies
6	220
7	2 485
8	34 300
9	559 405
10	10 525 900
11	224 449 225

n external particles \Rightarrow topologies for $n - 1$ particles needed

Topology generation in carlomat

of topologies grows dramatically with # of external particles.

# of particles	# of topologies
6	220
7	2 485
8	34 300
9	559 405
10	10 525 900
11	224 449 225

n external particles \Rightarrow topologies for $n - 1$ particles needed
 \Rightarrow Feynman rules checked while adding the n -th particle.

Topology generation in carlomat

of topologies grows dramatically with # of external particles.

# of particles	# of topologies
6	220
7	2 485
8	34 300
9	559 405
10	10 525 900
11	224 449 225

n external particles \Rightarrow topologies for $n - 1$ particles needed
 \Rightarrow Feynman rules checked while adding the n -th particle.

To facilitate this, each topology is divided into two parts, each being checked against the Feynman rules separately.

Topology generation in carlomat

of topologies grows dramatically with # of external particles.

# of particles	# of topologies
6	220
7	2 485
8	34 300
9	559 405
10	10 525 900
11	224 449 225

n external particles \Rightarrow topologies for $n - 1$ particles needed
 \Rightarrow Feynman rules checked while adding the n -th particle.

To facilitate this, each topology is divided into two parts, each being checked against the Feynman rules separately.

The particle mixing is added just at this stage.

Topology generation in carlomat

of topologies grows dramatically with # of external particles.

# of particles	# of topologies
6	220
7	2 485
8	34 300
9	559 405
10	10 525 900
11	224 449 225

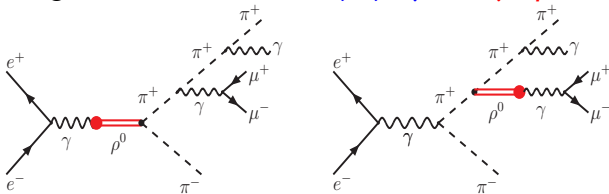
n external particles \Rightarrow topologies for $n - 1$ particles needed
 \Rightarrow Feynman rules checked while adding the n -th particle.

To facilitate this, each topology is divided into two parts, each being checked against the Feynman rules separately.

The particle mixing is added just at this stage.

q^2 -dependent mixing terms - example

Feynman diagrams of $e^+e^- \rightarrow \pi^+\pi^-\mu^+\mu^-\gamma$ with $\gamma-\rho^0$ mixing:

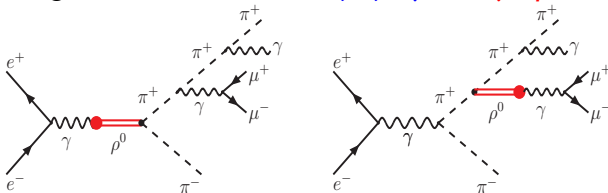


Two (three) particles are combined into the third (fourth) leg of a triple (quartic) Feynman vertex which is then folded with the adjacent Feynman propagator to form an off shell particle.

That is represented by an array of spinors, polarization vectors or scalars, with elements labelled with the polarization indices of spinors or polarization vectors of which it is formed.

q^2 -dependent mixing terms - example

Feynman diagrams of $e^+e^- \rightarrow \pi^+\pi^-\mu^+\mu^-\gamma$ with $\gamma-\rho^0$ mixing:



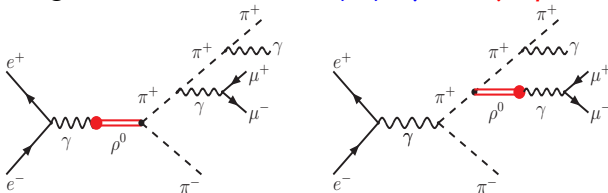
Two (three) particles are combined into the third (fourth) leg of a triple (quartic) Feynman vertex which is then folded with the adjacent Feynman propagator to form an off shell particle.

That is represented by an array of spinors, polarization vectors or scalars, with elements labelled with the polarization indices of spinors or polarization vectors of which it is formed.

If the particle mixing is present, the program checks whether the propagator of the off shell particle can be mixed or not, if so, a new off shell particle is formed.

q^2 -dependent mixing terms - example

Feynman diagrams of $e^+e^- \rightarrow \pi^+\pi^-\mu^+\mu^-\gamma$ with $\gamma-\rho^0$ mixing:



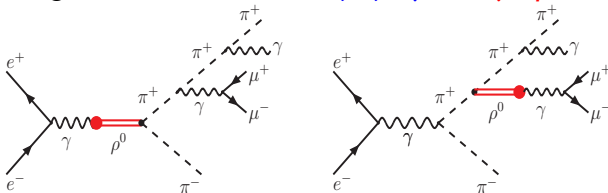
Two (three) particles are combined into the third (fourth) leg of a triple (quartic) Feynman vertex which is then folded with the adjacent Feynman propagator to form an off shell particle.

That is represented by an array of spinors, polarization vectors or scalars, with elements labelled with the polarization indices of spinors or polarization vectors of which it is formed.

If the particle mixing is present, the program checks whether the propagator of the off shell particle can be mixed or not, if so, a new off shell particle is formed. The particle with mixing is appropriately tagged in order not to be mixed again.

q^2 -dependent mixing terms - example

Feynman diagrams of $e^+e^- \rightarrow \pi^+\pi^-\mu^+\mu^-\gamma$ with $\gamma-\rho^0$ mixing:



Two (three) particles are combined into the third (fourth) leg of a triple (quartic) Feynman vertex which is then folded with the adjacent Feynman propagator to form an off shell particle.

That is represented by an array of spinors, polarization vectors or scalars, with elements labelled with the polarization indices of spinors or polarization vectors of which it is formed.

If the particle mixing is present, the program checks whether the propagator of the off shell particle can be mixed or not, if so, a new off shell particle is formed. The particle with mixing is appropriately tagged in order not to be mixed again.

To give a better control over the mixing contributions to a given process, subroutines `bbkk` and `bbmd` for computation of the helicity amplitudes of a building block or a complete Feynman diagram with mixing are equipped with the option:

`iwgt=0/1,2,...` if the additional complex factor c_1, c_2, \dots
is `not/is` to be included in $f_{AV}(q^2)$

q^2 -dependent mixing terms

The actual names for that option in `carlocom` are:

`imrho`, `imome`, `imphi`, `imrh1`, `imrh2` for $\rho^0, \omega, \phi, \rho_1, \rho_2$ meson, respectively.

The complex factor c_j , $j = 1, 2, \dots$ is given by

$$c_j = w_j e^{i\phi_j} f_j(q^2),$$

where w_j is a positive weight, ϕ_j is an angle in degrees, which should be both specified for each possible particle mixing term in the main program for the MC computation `carlocom`, and $f_j(q^2)$ is a possible four momentum transfer dependence that is defined in subroutine `weightfactor`.

q^2 -dependent mixing terms

The actual names for that option in `carlocom` are:

`imrho`, `imome`, `imphi`, `imrh1`, `imrh2` for $\rho^0, \omega, \phi, \rho_1, \rho_2$ meson, respectively.

The complex factor c_j , $j = 1, 2, \dots$ is given by

$$c_j = w_j e^{i\phi_j} f_j(q^2),$$

where w_j is a positive weight, ϕ_j is an angle in degrees, which should be both specified for each possible particle mixing term in the main program for the MC computation `carlocom`, and $f_j(q^2)$ is a possible four momentum transfer dependence that is defined in subroutine `weightfactor`.

Only three simple dependencies corresponding to `iwgt=1,2,3` are currently defined in `weightfactor`, but the user can easily add more options by implementing new

`else if (iwgt == ...) then` conditions.

q^2 -dependent mixing terms

The actual names for that option in `carlocom` are:

`imrho`, `imome`, `imphi`, `imrh1`, `imrh2` for $\rho^0, \omega, \phi, \rho_1, \rho_2$ meson, respectively.

The complex factor c_j , $j = 1, 2, \dots$ is given by

$$c_j = w_j e^{i\phi_j} f_j(q^2),$$

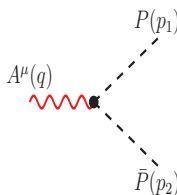
where w_j is a positive weight, ϕ_j is an angle in degrees, which should be both specified for each possible particle mixing term in the main program for the MC computation `carlocom`, and $f_j(q^2)$ is a possible four momentum transfer dependence that is defined in subroutine `weightfactor`.

Only three simple dependencies corresponding to `iwgt=1,2,3` are currently defined in `weightfactor`, but the user can easily add more options by implementing new

`else if (iwgt == ...) then` conditions.

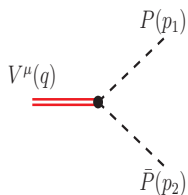
q^2 -dependent interaction vertices

Triple vertices of the form similar to those of sQED:



A Feynman diagram showing a triple vertex. On the left, a wavy red line representing a photon with momentum q and index μ , labeled $A^\mu(q)$, enters a black vertex. From this vertex, two dashed lines representing pseudoscalars emerge: one with momentum p_1 and index μ , labeled $P(p_1)$, and another with momentum p_2 and index μ , labeled $\bar{P}(p_2)$.

$$\equiv ief_{APP}(q^2)(p_1 - p_2)^\mu$$



A Feynman diagram showing a triple vertex. On the left, a double red line representing a vector meson with momentum q and index μ , labeled $V^\mu(q)$, enters a black vertex. From this vertex, two dashed lines representing pseudoscalars emerge: one with momentum p_1 and index μ , labeled $P(p_1)$, and another with momentum p_2 and index μ , labeled $\bar{P}(p_2)$.

$$\equiv if_{VPP}(q^2)(p_1 - p_2)^\mu$$

where $V = \rho^0, \omega, \phi$ and $P = \pi^+, K^+, K^0$.

q^2 -dependent interaction vertices

Triple vertices of a more complicated tensor form:

$$\pi^0(q) \text{ --- } \bullet \begin{cases} \nearrow A^\mu(p_1) \\ \searrow A^\nu(p_2) \end{cases} \equiv e^2 f_{\pi AA}(q^2) \varepsilon^{\mu\nu\alpha\beta} p_{1\alpha} p_{2\beta}$$

$$\pi^0(q) \text{ --- } \bullet \begin{cases} \nearrow A^\mu(p_1) \\ \searrow V^\nu(p_2) \end{cases} \equiv i e f_{\pi AV}(q^2) \varepsilon^{\mu\nu\alpha\beta} p_{1\alpha} p_{2\beta}$$

$$\pi^\mp(q) \text{ --- } \bullet \begin{cases} \nearrow A^\mu(p_1) \\ \searrow \rho^{\pm\nu}(p_2) \end{cases} \equiv i e f_{\pi^\mp A \rho^\pm}(q^2) \varepsilon^{\mu\nu\alpha\beta} p_{1\alpha} p_{2\beta}$$

$$P(q) \text{ --- } \bullet \begin{cases} \nearrow \omega^\mu(p_1) \\ \searrow V^\nu(p_2) \end{cases} \equiv f_{P\omega V}(q^2) \varepsilon^{\mu\nu\alpha\beta} p_{1\alpha} p_{2\beta}$$

where, in the top right corner, $V = \rho^0, \omega$, and in the bottom right corner $P = \pi^0$ and $V = \rho^0$ or $P = \pi^\mp$ and $V = \rho^\pm$.

q^2 -dependent interaction vertices

Quartic vertices of the HLS model:

$$\equiv 2ie f_{A\rho\pi\pi}(q^2)g^{\mu\nu}$$

$$\equiv 2if_{\rho\rho\pi\pi}(q^2)g^{\mu\nu}$$

$$\equiv -ef_{A\pi\pi\pi}(q^2)\varepsilon^{\mu\nu\alpha\beta}p_{1\nu}p_{2\alpha}p_{3\beta}$$

$$\equiv -ef_{\omega\pi\pi\pi}(q^2)\varepsilon^{\mu\nu\alpha\beta}p_{1\nu}p_{2\alpha}p_{3\beta}$$

The vertices in the first row have the same tensor form as the quartic vertex of the sQED or the quartic vertices of the Nambu-Goldstone boson – gauge boson interaction of the SM, which were implemented already in the first version of carlomat.

New program options

All subroutines that are used to compute the building blocks or the complete helicity amplitudes of the Feynman diagrams containing vertices of the HLS model have been supplied with **the running coupling option**.

The options are to be specified in subroutine `couplsm`, where they are defined below the assignment for each particular coupling.

```
icoupl_name=0/1,2,... if the fixed/running coupling  
is to be used in the computation,  
where choices 1,2,... corresponding to different running  
couplings  $f_{..}(q^2)$  should be added by the user as extra  
else if (ig == ...) then blocks in subroutine runcoupl.
```

New program options

All subroutines that are used to compute the building blocks or the complete helicity amplitudes of the Feynman diagrams containing vertices of the HLS model have been supplied with **the running coupling option**.

The options are to be specified in subroutine `couplsm`, where they are defined below the assignment for each particular coupling.

`icoupl_name=0/1,2,...` if the **fixed/running coupling** is to be used in the computation, where choices `1,2,...` corresponding to different **running couplings** $f_{..}(q^2)$ should be added by the user as extra `else if (ig == ...) then` blocks in subroutine `runcoupl`.

The four momentum transfer q is determined automatically from the four momentum conservation in the corresponding interaction vertex at the stage of code generation.

New program options

All subroutines that are used to compute the building blocks or the complete helicity amplitudes of the Feynman diagrams containing vertices of the HLS model have been supplied with **the running coupling option**.

The options are to be specified in subroutine `couplsm`, where they are defined below the assignment for each particular coupling.

`icoupl_name=0/1,2,...` if the **fixed/running coupling** is to be used in the computation, where choices `1,2,...` corresponding to different **running couplings** $f_{..}(q^2)$ should be added by the user as extra `else if (ig == ...) then` blocks in subroutine `runcoupl`.

The four momentum transfer q is determined automatically from the four momentum conservation in the corresponding interaction vertex at the stage of code generation.

New program options

Many couplings of the $R\chi T$ or HLS model are not known well enough and must be adjusted in consecutive runs of the program in order to obtain satisfactory description of the experimental data. If there are no hints as to the form of the running couplings $f_{\dots}(q^2)$ then it is recommended to set the corresponding running coupling option to 0, which means that the fixed coupling is to be used in the computation.

New program options

Many couplings of the $R\chi T$ or HLS model are not known well enough and must be adjusted in consecutive runs of the program in order to obtain satisfactory description of the experimental data. If there are no hints as to the form of the running couplings $f_{\dots}(q^2)$ then it is recommended to set the corresponding running coupling option to 0, which means that the fixed coupling is to be used in the computation.

The user can also modify any of the fixed couplings by changing the corresponding assignments in `couplsm`, where the couplings are defined in terms of the physical parameters of module `inprms`.

New program options

Many couplings of the $R\chi T$ or HLS model are not known well enough and must be adjusted in consecutive runs of the program in order to obtain satisfactory description of the experimental data. If there are no hints as to the form of the running couplings $f_{\dots}(q^2)$ then it is recommended to set the corresponding running coupling option to 0, which means that the fixed coupling is to be used in the computation.

The user can also modify any of the fixed couplings by changing the corresponding assignments in `couplsm`, where the couplings are defined in terms of the physical parameters of module `inprms`.

The main part of the MC computation program `carlocom` contains also a few flags: `iarho`, `iaome`, `iaphi`, `iarho1` and `iarho2` that allow to switch off and on the photon mixing with ρ, ω, ϕ , ρ_1 and ρ_2 vector mesons without a need of running the code generation program anew, provided that the corresponding mixing terms were included in a file `vertices.dat` when the MC code was generated.

New program options

Many couplings of the $R\chi T$ or HLS model are not known well enough and must be adjusted in consecutive runs of the program in order to obtain satisfactory description of the experimental data. If there are no hints as to the form of the running couplings $f_{\dots}(q^2)$ then it is recommended to set the corresponding running coupling option to 0, which means that the fixed coupling is to be used in the computation.

The user can also modify any of the fixed couplings by changing the corresponding assignments in `couplsm`, where the couplings are defined in terms of the physical parameters of module `inprms`. The main part of the MC computation program `carlocom` contains also a few flags: `iarho`, `iaome`, `iaphi`, `iarho1` and `iarho2` that allow to switch off and on the photon mixing with ρ, ω, ϕ , ρ_1 and ρ_2 vector mesons without a need of running the code generation program anew, provided that the corresponding mixing terms were included in a file `vertices.dat` when the MC code was generated.

New program options

The subroutines for computation of the four vectors representing vector mesons have been in addition supplied with the **running width option** `iwidth_name`, i.e. `igmrh`, `igmom`, `igmph`, `igmr1`, `igmr2` for the running width of ρ^0 , ω , ϕ , ρ_1 , ρ_2 , respectively.

`iwidth_name=0/1,2,3` if the **fixed/running** width of the vector particle should be used,

where choices **1,2,3** refer to different **running width options** in subroutine `runwidth` which again can easily be extended by the user. The options are controlled from `carlocom`, the main part of the MC computation program.

An important new option in the program that allows to test the EM gauge invariance for processes with one or more external photons is `igauge` in `carlcom.f`:

`igauge=1,2,.../else` if the gauge invariance `is/is not` to be tested,

where `1,2,...` is the number of a photon, counting from left to right, whose polarization four vector is replaced with its four momentum.

EM gauge invariance tests

The cross sections in pb at $\sqrt{s} = 1$ GeV **without** and **with** contribution from the $\pi^\mp\gamma\rho^\pm$ vertices with the following cuts:

$$\theta_{\gamma l} > 5^\circ, \quad \theta_{\gamma\pi} > 5^\circ, \quad E_\gamma > 10 \text{ MeV}.$$

igauge	$\sigma(e^+e^- \rightarrow \pi^+\pi^-\pi^+\pi^-\gamma)$		$\sigma(e^+e^- \rightarrow \pi^+\pi^-\mu^+\mu^-\gamma)$	
0	11.86(5)	11.83(5)	0.0590(2)	0.0586(2)
1	0.124(2)e-30	0.441(1)e-10	0.636(9)e-33	0.973(1)e-9

The numbers in parentheses show the MC uncertainty of the last decimal.

The inclusion of the $\pi^\mp\gamma\rho^\pm$ vertices spoils the EM gauge invariance. The effect is not practically relevant, but in some phase space regions it may become sizable.

EM gauge invariance tests

The cross sections in pb at $\sqrt{s} = 1$ GeV **without** and **with** contribution from the $\pi^\mp\gamma\rho^\pm$ vertices with the following cuts:

$$\theta_{\gamma l} > 5^\circ, \quad \theta_{\gamma\pi} > 5^\circ, \quad E_\gamma > 10 \text{ MeV}.$$

igauge	$\sigma(e^+e^- \rightarrow \pi^+\pi^-\pi^+\pi^-\gamma)$		$\sigma(e^+e^- \rightarrow \pi^+\pi^-\mu^+\mu^-\gamma)$	
0	11.86(5)	11.83(5)	0.0590(2)	0.0586(2)
1	0.124(2)e-30	0.441(1)e-10	0.636(9)e-33	0.973(1)e-9

The numbers in parentheses show the MC uncertainty of the last decimal.

The inclusion of the $\pi^\mp\gamma\rho^\pm$ vertices spoils the EM gauge invariance. The effect is not practically relevant, but in some phase space regions it may become sizable.

Running time:

EM gauge invariance tests

The cross sections in pb at $\sqrt{s} = 1$ GeV **without** and **with** contribution from the $\pi^\mp \gamma \rho^\pm$ vertices with the following cuts:

$$\theta_{\gamma l} > 5^\circ, \quad \theta_{\gamma\pi} > 5^\circ, \quad E_\gamma > 10 \text{ MeV}.$$

igauge	$\sigma(e^+e^- \rightarrow \pi^+\pi^-\pi^+\pi^-\gamma)$		$\sigma(e^+e^- \rightarrow \pi^+\pi^-\mu^+\mu^-\gamma)$	
0	11.86(5)	11.83(5)	0.0590(2)	0.0586(2)
1	0.124(2)e-30	0.441(1)e-10	0.636(9)e-33	0.973(1)e-9

The numbers in parentheses show the MC uncertainty of the last decimal.

The inclusion of the $\pi^\mp \gamma \rho^\pm$ vertices spoils the EM gauge invariance. The effect is not practically relevant, but in some phase space regions it may become sizable.

Running time: the code generation for both processes takes a fraction of a second time.

EM gauge invariance tests

The cross sections in pb at $\sqrt{s} = 1$ GeV **without** and **with** contribution from the $\pi^\mp\gamma\rho^\pm$ vertices with the following cuts:

$$\theta_{\gamma l} > 5^\circ, \quad \theta_{\gamma\pi} > 5^\circ, \quad E_\gamma > 10 \text{ MeV}.$$

igauge	$\sigma(e^+e^- \rightarrow \pi^+\pi^-\pi^+\pi^-\gamma)$		$\sigma(e^+e^- \rightarrow \pi^+\pi^-\mu^+\mu^-\gamma)$	
0	11.86(5)	11.83(5)	0.0590(2)	0.0586(2)
1	0.124(2)e-30	0.441(1)e-10	0.636(9)e-33	0.973(1)e-9

The numbers in parentheses show the MC uncertainty of the last decimal.

The inclusion of the $\pi^\mp\gamma\rho^\pm$ vertices spoils the EM gauge invariance. The effect is not practically relevant, but in some phase space regions it may become sizable.

Running time: the code generation for both processes takes a fraction of a second time. The MC computation with 10×200000 calls takes 142s and 43s time for $\pi^+\pi^-\pi^+\pi^-\gamma$ and $\pi^+\pi^-\mu^+\mu^-\gamma$ final states on processor Intel^R CoreTM i5-4200M CPU @ 2.50 GHz with a 64 bit Intel Fortran compiler.

EM gauge invariance tests

The cross sections in pb at $\sqrt{s} = 1$ GeV **without** and **with** contribution from the $\pi^\mp\gamma\rho^\pm$ vertices with the following cuts:

$$\theta_{\gamma l} > 5^\circ, \quad \theta_{\gamma\pi} > 5^\circ, \quad E_\gamma > 10 \text{ MeV}.$$

igauge	$\sigma(e^+e^- \rightarrow \pi^+\pi^-\pi^+\pi^-\gamma)$		$\sigma(e^+e^- \rightarrow \pi^+\pi^-\mu^+\mu^-\gamma)$	
0	11.86(5)	11.83(5)	0.0590(2)	0.0586(2)
1	0.124(2)e-30	0.441(1)e-10	0.636(9)e-33	0.973(1)e-9

The numbers in parentheses show the MC uncertainty of the last decimal.

The inclusion of the $\pi^\mp\gamma\rho^\pm$ vertices spoils the EM gauge invariance. The effect is not practically relevant, but in some phase space regions it may become sizable.

Running time: the code generation for both processes takes a fraction of a second time. The MC computation with 10×200000 calls takes 142s and 43s time for $\pi^+\pi^-\pi^+\pi^-\gamma$ and $\pi^+\pi^-\mu^+\mu^-\gamma$ final states on processor Intel^R CoreTM i5-4200M CPU @ 2.50 GHz with a 64 bit Intel Fortran compiler.

EM interaction of nucleons

The effective Lagrangian of the Wtb interaction containing operators of dimension four and five has the following form:

$$L_{Wtb} = \frac{g}{\sqrt{2}} V_{tb} \left[W_{\mu}^{-} \bar{b} \gamma^{\mu} \left(f_1^L P_L + f_1^R P_R \right) t - \frac{1}{m_W} \partial_{\nu} W_{\mu}^{-} \bar{b} \sigma^{\mu\nu} \left(f_2^L P_L + f_2^R P_R \right) t \right] + \text{h.c.}$$

Couplings $f_i^L, f_i^R, i = 1, 2$, can be complex in general. In the SM, $f_1^L = 1$ and other couplings are 0.

The EM interaction of spin 1/2 nucleons has a similar form:

$$L_{\gamma NN} = e A_{\mu} \bar{N}(p') \left[\gamma^{\mu} F_1(Q^2) + \frac{i}{2m_N} \sigma^{\mu\nu} q_{\nu} F_2(Q^2) \right] N(p).$$

Form factors $F_1(Q^2)$ and $F_2(Q^2)$, where $Q^2 = -(p - p')^2$, have been adopted from PHOKARA. [Thanks to S. Tracz and H. Czyż.]

EM interaction of nucleons

The effective Lagrangian of the Wtb interaction containing operators of dimension four and five has the following form:

$$L_{Wtb} = \frac{g}{\sqrt{2}} V_{tb} \left[W_{\mu}^{-} \bar{b} \gamma^{\mu} \left(f_1^L P_L + f_1^R P_R \right) t - \frac{1}{m_W} \partial_{\nu} W_{\mu}^{-} \bar{b} \sigma^{\mu\nu} \left(f_2^L P_L + f_2^R P_R \right) t \right] + \text{h.c.}$$

Couplings $f_i^L, f_i^R, i = 1, 2$, can be complex in general. In the SM, $f_1^L = 1$ and other couplings are 0.

The EM interaction of spin 1/2 nucleons has a similar form:

$$L_{\gamma NN} = e A_{\mu} \bar{N}(p') \left[\gamma^{\mu} F_1(Q^2) + \frac{i}{2m_N} \sigma^{\mu\nu} q_{\nu} F_2(Q^2) \right] N(p).$$

Form factors $F_1(Q^2)$ and $F_2(Q^2)$, where $Q^2 = -(p - p')^2$, have been adopted from PHOKARA. [Thanks to S. Tracz and H. Czyż.]

⇒ Simulation of processes involving the EM interaction of nucleons.

EM interaction of nucleons

The effective Lagrangian of the Wtb interaction containing operators of dimension four and five has the following form:

$$L_{Wtb} = \frac{g}{\sqrt{2}} V_{tb} \left[W_{\mu}^{-} \bar{b} \gamma^{\mu} \left(f_1^L P_L + f_1^R P_R \right) t - \frac{1}{m_W} \partial_{\nu} W_{\mu}^{-} \bar{b} \sigma^{\mu\nu} \left(f_2^L P_L + f_2^R P_R \right) t \right] + \text{h.c.}$$

Couplings $f_i^L, f_i^R, i = 1, 2$, can be complex in general. In the SM, $f_1^L = 1$ and other couplings are 0.

The EM interaction of spin 1/2 nucleons has a similar form:

$$L_{\gamma NN} = e A_{\mu} \bar{N}(p') \left[\gamma^{\mu} F_1(Q^2) + \frac{i}{2m_N} \sigma^{\mu\nu} q_{\nu} F_2(Q^2) \right] N(p).$$

Form factors $F_1(Q^2)$ and $F_2(Q^2)$, where $Q^2 = -(p - p')^2$, have been adopted from PHOKARA. [Thanks to S. Tracz and H. Czyż.]

⇒ Simulation of processes involving the EM interaction of nucleons.

Restrictions

As in previous versions of the program the number of particles in the final state is **limited to 10** which exceeds typical numbers of particles observed in the exclusive low energy e^+e^- -annihilation processes.

However, in the presence of photon–vector meson mixing, the Feynman diagrams proliferate, for example, with currently implemented Feynman rules, there are 90672 diagrams of $e^+e^- \rightarrow 3(\pi^+\pi^-)$.

⇒ The compilation time of generated code may become very long already for processes with smaller number of the final state particles.

Restrictions

As in previous versions of the program the number of particles in the final state is **limited to 10** which exceeds typical numbers of particles observed in the exclusive low energy e^+e^- -annihilation processes.

However, **in the presence of photon–vector meson mixing, the Feynman diagrams proliferate, for example,** with currently implemented Feynman rules, **there are 90672 diagrams of $e^+e^- \rightarrow 3(\pi^+\pi^-)$.**

⇒ The compilation time of generated code may become very long already for processes with smaller number of the final state particles.

Many couplings of the effective models are not known well enough and must be adjusted in consecutive runs of the program in order to obtain satisfactory description of the experimental data.

Restrictions

As in previous versions of the program the number of particles in the final state is **limited to 10** which exceeds typical numbers of particles observed in the exclusive low energy e^+e^- -annihilation processes.

However, **in the presence of photon–vector meson mixing, the Feynman diagrams proliferate, for example,** with currently implemented Feynman rules, **there are 90672 diagrams of $e^+e^- \rightarrow 3(\pi^+\pi^-)$.**

⇒ The compilation time of generated code may become very long already for processes with smaller number of the final state particles.

Many couplings of the effective models are not known well enough and must be adjusted in consecutive runs of the program in order to obtain satisfactory description of the experimental data.

Thank you for your attention